JOURNAL OF PROPULSION AND POWER
Vol. 23, No. 6, November–December 2007

Impeller–Diffuser Interaction in Centrifugal Compressors: Numerical Analysis of Radiver Test Case

P. Boncinelli*
University of Florence, 50012 Florence, Italy
M. Ermini† and S. Bartolacci†
General Electric Oil & Gas, Nuovo Pignone, 50127 Florence, Italy
and
A. Arnone‡
Sergio Stecco Department of Energy Engineering, University of Florence, 50139 Florence, Italy

DOI: 10.2514/1.27028

In the present work, a numerical analysis of the Radiver test case was carried out using computational fluid dynamics techniques. Radiver is a centrifugal compressor stage for which a large amount of experimental data are available for ten diffuser configurations. Two diffuser geometries, differing in the radial gap between impeller exit and diffuser inlet, were compared to investigate the impact of impeller–diffuser interaction on the stage performance and the flowfield. Both steady and unsteady computations were carried out with the aim of separating unsteady effects from steady ones. As a result, flow unsteadiness turned out to have a positive impact on the sole lower radial gap configuration, especially in terms of the flow structure, in agreement with experimental indications. Moreover, physical mechanisms responsible for this behavior were identified and discussed.

Nomenclature

$\boldsymbol{c}$	=	velocity vector
$G2$	=	diffuser geometry 2
$G5$	=	diffuser geometry 5
$\dot{m}_{\text{red}}$	=	corrected mass flow, kg/s (International Standard Atmosphere inlet conditions: $p_{0I} = 1.013$ bar, $T_{0I} = 288.15$ K)
$\boldsymbol{n}$	=	unit vector
r	=	radius, mm
r_4/r_2	=	radial gap
$\alpha_{4\text{SS}}$	=	diffuser vane leading edge angle, deg
ϕ/ϕ_{td}	=	nondimensional circumferential coordinate (diffuser pitch)
$2M$	=	measurement section at impeller exit/diffuser inlet
$7M$	=	measurement section at diffuser vane exit
$8M$	=	measurement section at diffuser exit

Subscripts

SS	=	suction side
2	=	impeller exit
4	=	diffuser vane inlet

I. Introduction

MODERN centrifugal compressors, both for aeronautical and industrial applications, exploit heavily loaded stages which allow one to obtain the required total pressure ratio while reducing the compressor size. Heavily loaded stages are typically characterized by transonic impellers coupled with vaned diffusers, which help the designer increase the stage performance [1–4].

The aerodynamic design of these stages is a nontrivial task to accomplish, due to the complexity of the flow evolving across stationary and rotating components. Moreover, the effectiveness of the design is determined by a correct matching between the impeller and the diffuser. This target cannot be fully achieved without accounting for impeller–diffuser interaction, which is known, in some instances, to have strong influence on both stage performance and flowfield. This interaction is geometry-dependent, as shown by Gottfried and Fleeter [5], with its intensity mainly related to the radial gap size between the impeller exit and the diffuser inlet. For example, results reported by Rodgers [6] and Clements and Artt [7] show the dependence of the stage total-to-static pressure ratio on the radial gap, thereby confirming the existence of an optimum value for it. More recently, analogous results were found in experiments performed on a centrifugal impeller coupled with a radial-vaned diffuser by Sanders and Fleeter [8]. A clear understanding of the flow physics involved in impeller–diffuser interaction is likely to lead to significant improvements in their integrated design (Shum et al. [9]). However, this goal is far from being fully achieved, so considerable efforts were and are currently being devoted to this challenge.

Nowadays, impeller–diffuser interaction can be evaluated both experimentally and numerically. As far as experimental investigations are concerned, many works are reported in literature. Filipenco et al. [10] and Deniz et al. [11] addressed the effect of different inlet profiles on radial diffusers performance. Unsteady flowfield measurements in the radial gap region were presented by Krain [12,13], Inoue and Cumpsty [14] and, more recently, by Ibaraki et al. [15]. However, experimental investigations provide the designer with the global effect of the interaction, but are not capable of isolating all aspects related to the influence of the impeller on the diffuser and vice versa. Currently, evaluating the relative importance of each aspect is necessary for improving the comprehension of the involved physical mechanisms.

Numerical computations make it possible to do this, because both steady and time-accurate analyses can be performed. Sanders and Fleeter [16] developed an unsteady aerodynamic model to predict the response of both axial- and radial-flow turbomachinery blading resulting from potential field interactions. Moreover, investigations

Presented as Paper 3453 at the 25th AIAA Aerodynamic Measurement Technology and Ground Testing Conference, San Francisco, California, 5–8 June 2006; received 4 August 2006; revision received 11 July 2007; accepted for publication 28 July 2007.

*Research Fellow, Department of Agricultural and Forestry Engineering–Mechanics Section, Piazzale delle Cascine, 15-50144.

†Design Engineer, Centrifugal Compressor Division, General Electric Oil & Gas, Nuovo Pignone, Via F. Matteucci, 2-50127.

‡Professor, Sergio Stecco Department of Energy Engineering, Via S. Marta, 3-50139.

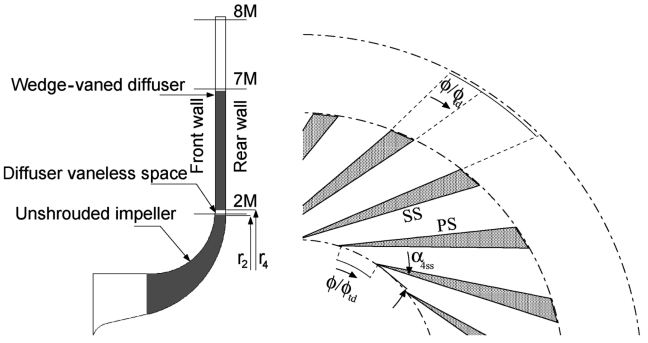

a) Meridional view b) Diffuser blade-to-blade view

Fig. 1 Geometrical configuration and measurement sections of the Radiver centrifugal compressor stage.

Table 1 Main technical data of the Radiver stage

Physical elements	
Compressor	
Evolving fluid	air
Inlet total pressure, bar	0.6
Inlet total temperature, K	296.0
Nominal shaft speed, rpm	35,200
Impeller	
Exit radius r_2, mm	135
Blade backsweep angle, deg	38
Number of blades	15
Diffuser	
Leading-edge angle α_{4SS}, deg	16.5
Height, mm	11.1
Exit radius, mm	345
Number of vanes	23

on different impeller–diffuser configurations using computational fluid dynamics (CFD) are provided, among others, by Shum et al. [9] and Peeters and Sleiman [17], who give evidence of the importance of unsteady effects. CFD capability of exploring flow structure details, which are difficult, expensive, and time-consuming to obtain by means of measurements, allows one to identify the main mechanisms associated with the interaction, and offers support to the analysis of experimental results. On the other hand, the availability of detailed experimental data is essential to assess numerical predictions. However, in open literature, there is a lack of both geometrical configurations and detailed measurements for extensive comparisons to numerical results.

For this reason, the open test case "Radiver," proposed by Ziegler et al. [18,19] and Ziegler [20], is a particularly attractive case to tackle. Radiver is a centrifugal compressor stage composed of an unshrouded impeller and a wedge-type diffuser, for which an extensive test series of measurements by using both steady probes and time-resolving laser-2-focus velocimeter are available. Experimental investigation was focused on achieving a better comprehension of impeller–diffuser interaction related to variations of both the radial gap and the diffuser vane angle. Measurements were performed at the Institute of Jet Propulsion and Turbomachinery at RWTH Aachen University in Germany. Part of the investigation was funded by the Deutsche Forschungsgemeinschaft (DFG). The experimental results were published as an open CFD test case. From experiments, impeller–diffuser interaction, depending largely on the radial gap, turned out to affect significantly the flow configuration in the diffuser channel. As a consequence, as suggested by Ziegler et al. [18,19] themselves, numerical investigations on the Radiver stage should mainly concentrate their efforts on unsteady computations, because a steady analysis would hardly be capable of correctly predicting the flowfield in the diffuser. To the authors' knowledge, no numerical work engaging this challenge has been published yet.

In the present work, a numerical analysis of the Radiver stage was carried out exploiting CFD techniques. Two diffuser geometries, differing in the radial gap between impeller exit and diffuser inlet, were compared by means of both steady and unsteady computations. The following goals were pursued:

1) Compare numerical results with experimental ones to assess numerical predictions.

2) Isolate and evaluate the impact of both steady and unsteady effects on stage performance and flowfield details.

3) Identify and understand the physical mechanisms by which interaction influences the performance and the flowfield.

This paper is arranged as follows. A short description of the stage configuration and the numerical approach is first provided. Then, the preceding goals are addressed in sequence through the presentation and discussion of the computational results. Finally, the main conclusions are stated.

II. Stage Configuration

The Radiver stage is characterized by a 15-blade unshrouded centrifugal impeller and a 23-vane wedge-type diffuser. Ten different diffuser geometries were experimentally investigated, varying both the radial gap between impeller exit and diffuser inlet, and the diffuser vane angle. A complete description of all geometrical configurations, the test rig setup, and operating conditions is provided by Ziegler et al. [18,19]. A schematic view of the stage, together with positions of the measurement sections $2M$, $7M$, and $8M$, is reported in Figs. 1a and 1b. Some technical data are summarized in Table 1.

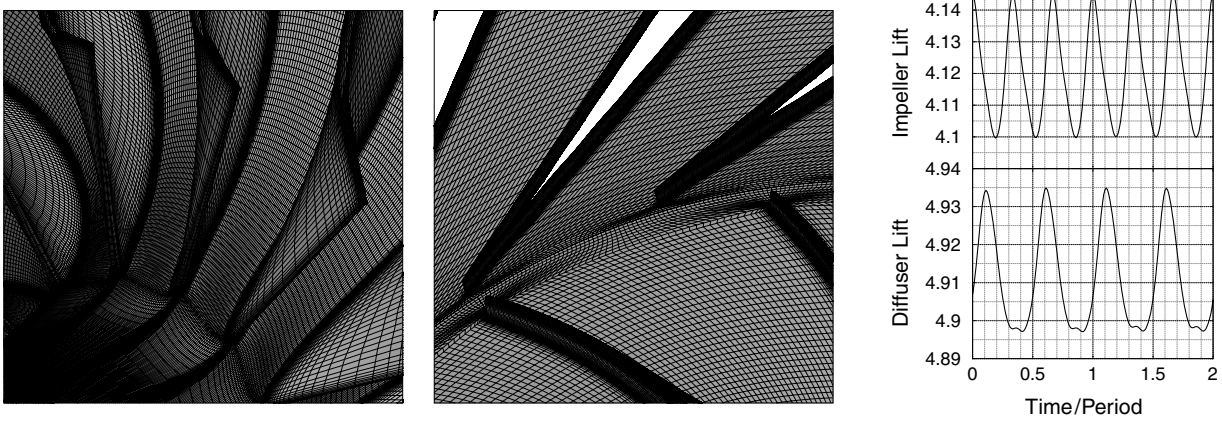

a) Impeller inlet b) Impeller exit - diffuser inlet c) Unsteady lift evolution

Fig. 2 Details of the computational grid and typical unsteady lift evolution.

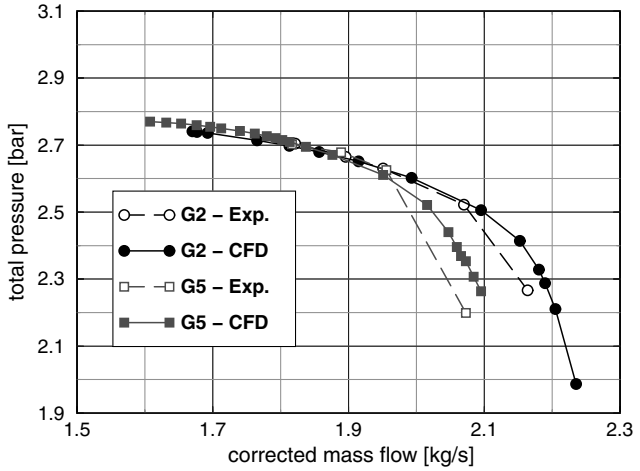

a) Section 7M

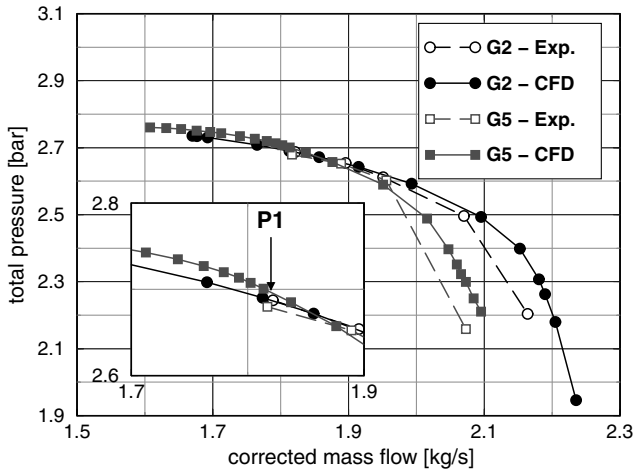

b) Section 8M

Fig. 3 Comparison between experimental and numerical total pressure vs corrected mass flow at sections 7*M* and 8*M* (steady analysis, experimental configuration).

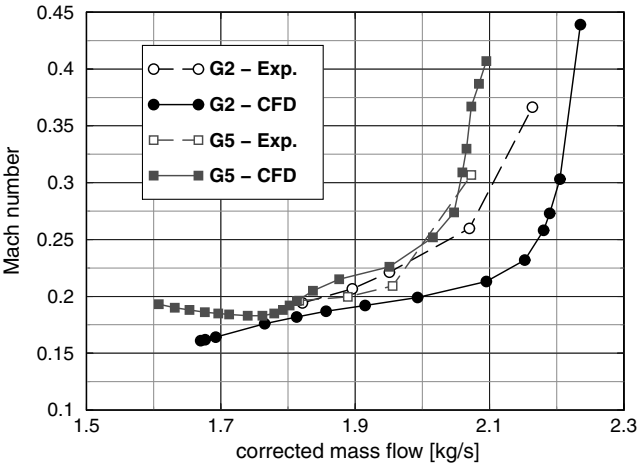

a) Section 7M

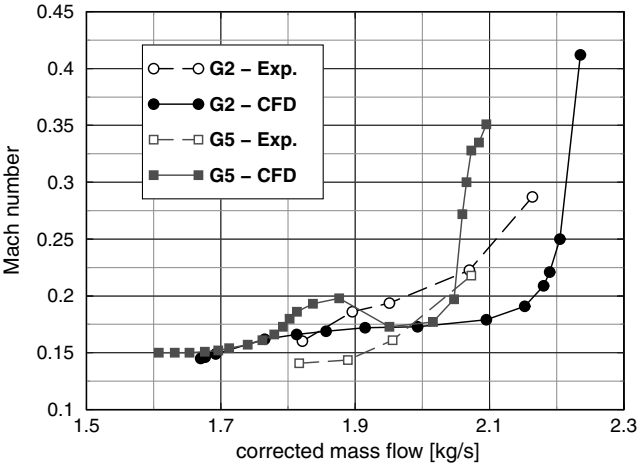

b) Section 8M

Fig. 4 Comparison between experimental and numerical Mach number vs corrected mass flow at sections 7*M* and 8*M* (steady analysis, experimental configuration).

In the present numerical analysis, two diffuser geometries were selected, characterized by fixed diffuser leading-edge angle ($\alpha_{4SS} = 16.5$ deg) and different values of the radial gap r_4/r_2: $r_4/r_2 = 1.14$ ($G2$) and $r_4/r_2 = 1.04$ ($G5$). Actually, from experimental results, the most significant differences in the impact of impeller–diffuser interaction are expected for these geometries, for which a larger amount of experimental data were available, too.

III. Numerical Procedure

Computations were performed using the TRAF code. TRAF is a three-dimensional, steady/unsteady, viscous, multigrid, multirow solver for the aerodynamic analysis of turbomachinery flows developed at the University of Florence, Italy. The numerical method used by the TRAF code is described in detail in Arnone et al. [21] and Arnone [22]. The space discretization is based on a cell-centered finite volume scheme. The system of governing equations is advanced in time using an explicit four-stage Runge–Kutta scheme. Residual smoothing, local time-stepping, and multigridding are employed to speed up convergence to the steady-state solution. A dual-time-stepping method [23,24] is used to perform time-accurate calculations. Both algebraic [25,26] and multi-equation [27,28] models are available for turbulence closure. In the present work, the Baldwin–Lomax model was employed, assuming a fully turbulent flow all over the wall surfaces, so that transition effects were neglected. Both impeller and diffuser blade rows were analyzed using H-type grids. Grid sizes were chosen to accomplish two opposite requirements: to compute solutions which are grid independent, and to manage computational times and costs. After some preliminary tests, two grid blocks sizing about 600,000 and 490,000 cells were used for solving the flow inside the impeller blade and the diffuser vane passages, respectively. This was judged to be an acceptable compromise, relying on experience (Arnone et al. [29], Bonaiuti et al. [1]), with a grid resolution near the walls corresponding approximately to $y^+ \approx 1$. Details of three-dimensional grids at the impeller inlet and in the radial gap region are illustrated in Figs. 2a and 2b. The tip clearance region was not gridded, assuming periodicity of flow quantities through the tip gap. Hot-running conditions were considered for setting the clearance height, as reported by Ziegler [20] and Weiss et al. [30].

Steady computations were performed on a single blade passage. Coupling between rows was achieved by using a mixing plane, which is handled by keeping the radial distribution of physical quantities (total quantities and flow angles at the inlet, static pressure at the outlet) while area averaging in the circumferential direction ("pitch averaging"). The same radial location of the mixing plane at $r/r_2 = 1.02$ was used for both $G2$ and $G5$ geometries. For each computation, convergence was assumed when a steady value of the rms of the residuals was reached, with at least a four-order magnitude reduction with respect to its initial value. This convergence criterion was found to satisfy the global balance of the mass flow rate across rows within about 0.1%.

In unsteady computations, the fact that the impeller and the diffuser have a different number of blades was addressed by

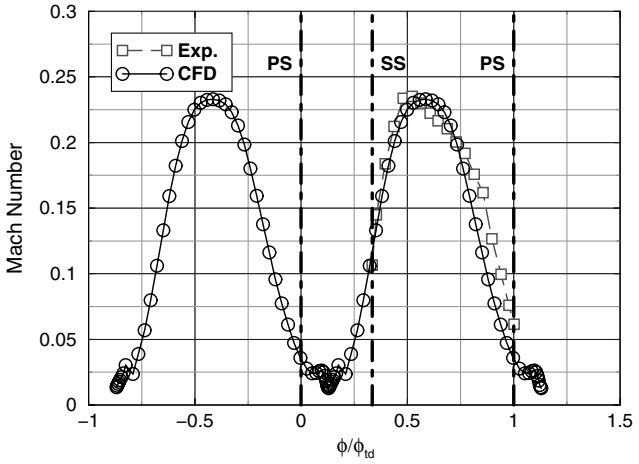

a) Section 7M – G2

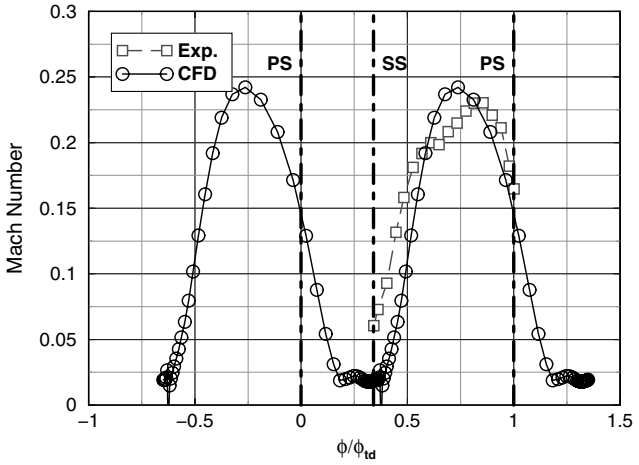

b) Section 7M – G5

Fig. 5 Comparison between experimental and numerical pitchwise distributions of spanwise-averaged Mach number at section 7*M* (P1, steady analysis, experimental configuration).

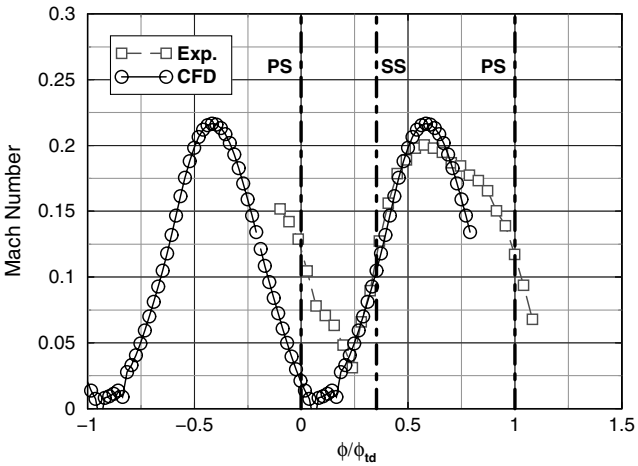

a) Section 8M – G2

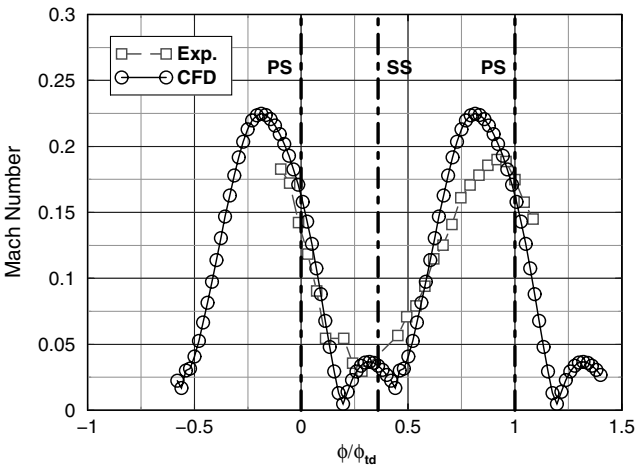

b) Section 8M – G5

Fig. 6 Comparison between experimental and numerical pitchwise distributions of spanwise-averaged Mach number at section 8*M* (P1, steady analysis, experimental configuration).

including several blade passages in the calculation. Communications between rows were obtained by means of a common interface plane (Fig. 2b). The same cell distribution in the spanwise direction was used for the two grids, whereas the circumferential match was provided through a linear interpolation of the flow variable values. To reduce computational costs and times, a ratio of two impeller blades to three diffuser vanes (14:21 blade ratio) was used to approximate the original 15:23 blade ratio. The 14:21 and 15:23 configurations will be from now on referred to as the "approximate" and "experimental" configurations, respectively. As for grid sizes, the two opposing requirements of numerical accuracy and reasonable computational times had to be weighed in choosing the number of time steps to discretize a period, defined as the time needed by the two impeller blades to cross the three diffuser vanes. In the present application, 100 time steps per period were used, according to experience on a similar stage configuration (Bonaiuti et al. [1]). The unsteady lift evolution on both the impeller and the diffuser was monitored during calculations. This parameter has proved to be a very effective one in evaluating the level of periodicity of the whole numerical solution (Arnone and Pacciani [24]). About 100 periods were needed to achieve a good level of periodicity. Figure 2c shows the unsteady lift evolution of the impeller and the diffuser for the last two periods.

IV. Results

The following numerical analyses were carried out on both *G*2 and *G*5 geometries: 1) a steady analysis on the experimental configuration, to compare numerical results with experimental ones (goal no. 1) (as described in Sec. IV.A); 2) steady and unsteady analyses on the approximate configuration to separate steady effects from unsteady ones, and investigate the physical mechanisms by which interaction affects the stage performance and flowfield (goals no. 2 and 3) (as described in Sec. IV.B).

All computations were performed at 80% nominal shaft speed. Steady computations covered the whole operating range of the stage reproducing test rig conditions to compare experimental and numerical characteristic curves. Then, the stage peak efficiency condition, referred as the "P1" operating point, corresponding to a corrected mass flow rate of about 1.81 kg/s, was considered. Time-consuming unsteady computations were carried out for a couple of operating points, including the P1 point, which was investigated in detail. Only time-averaged quantities are shown here. Analysis of the results was focused on understanding the effect of impeller–diffuser interaction on the diffuser performance.

A. Steady Analysis, Experimental Configuration

Computed characteristic curves of mass-averaged total pressure and Mach number at sections 7*M* and 8*M* are compared with experimental ones in Figs. 3 and 4 for both *G*2 and *G*5 geometries.

As far as total pressure is concerned (Fig. 3), the agreement is quite good all over the operating envelope at both sections. Small differences are observed at higher flow rates. A similar behavior was observed for static pressure curves, not reported here. At P1, the computed total pressure for *G*5 at section 8*M* is slightly higher than

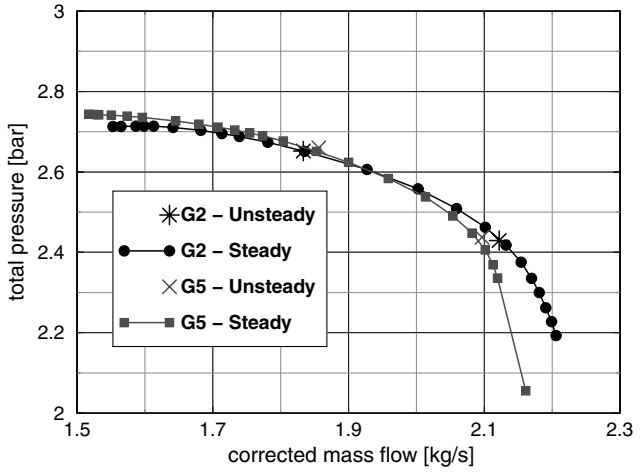

a) Section 7M

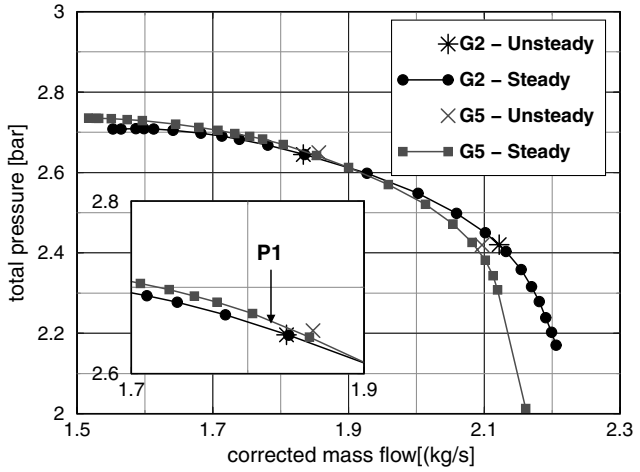

b) Section 8M

Fig. 7 Comparison between computed steady and time-averaged unsteady total pressure vs corrected mass flow at sections 7*M* and 8*M* (approximate configuration).

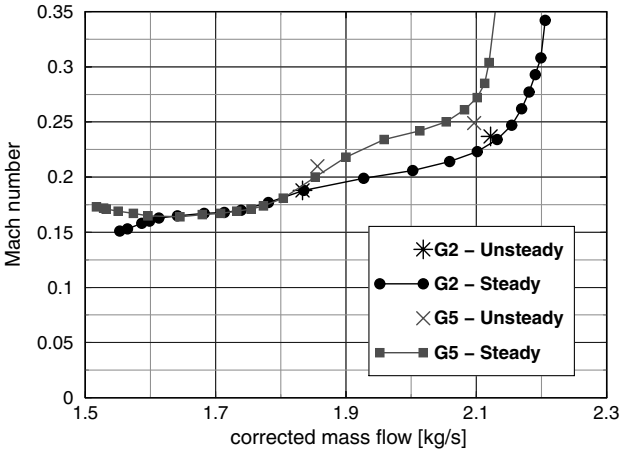

a) Section 7M

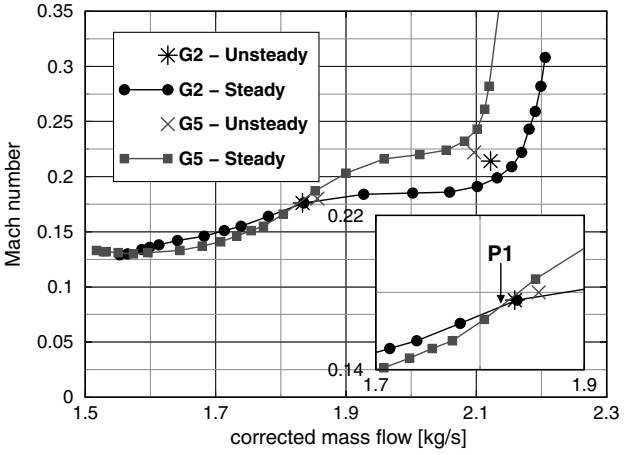

b) Section 8M

Fig. 8 Comparison between computed steady and time-averaged unsteady Mach number vs corrected mass flow at sections 7*M* and 8*M* (approximate configuration).

the corresponding one for *G*2, as highlighted in Fig. 3b. In both geometries, steady results overpredict the stall inception of the stage.

In Mach number curves, an opposite trend is observed comparing numerical and experimental results for *G*2 and *G*5 (Fig. 4). In particular, at section 8*M* and operating point P1, the computed mass-averaged Mach number is significantly higher for *G*5 than for *G*2 (Fig. 4b), whereas the opposite result was found by experiments. Similar numerical results were obtained by using different average criteria, such as area average. For this reason, computations do not support the conclusion, stated by Ziegler et al. [18], that the better performance experimentally observed at the collector exit for *G*5 is determined by lower Mach number levels at section 8*M*.

In Figs. 5 and 6, computed pitchwise distributions of spanwise mass-averaged Mach number at sections 7*M* and 8*M* for *G*2 and *G*5 are compared with experimental data at the P1 operating point. Blade pressure and suction side are referred here and will be from now on referred to as PS and SS. At section 7*M*, the agreement is quite good for *G*2 (Fig. 5a), whereas small differences are observed in *G*5 in terms of the shape near the peak of the distribution (Fig. 5b). At section 8*M*, differences are more pronounced. Considering *G*2 (Fig. 6a), peak values are similar, whereas the experimental wake width is significantly smaller. On the contrary, major discrepancies are observed in the peak region for *G*5 (Fig. 6b). Pitchwise total pressure distributions, not reported here for the sake of conciseness, suggest similar observations.

As a general consideration, from comparisons between experiments and computations, a reduction either in the maximum-to-minimum variation or in the wake width was observed at 8*M* in measured distributions with respect to computed ones, for both *G*2 and *G*5. This result would suggest that an enhanced mixing occurs in experiments between sections 7*M* and 8*M*.

B. Steady/Unsteady Analysis, Approximate Configuration

To separate unsteady effects from steady ones, results of steady and unsteady computations must be compared for the same stage configuration. However, as previously mentioned, the numerical approach adopted to perform unsteady computations requires an alteration of the blade ratio. As a consequence, a direct comparison with steady results obtained for the experimental configuration is not exact. For this reason, steady computations were also performed on the approximate configuration for *G*2 and *G*5 geometries, and results were compared with unsteady ones at the same flow rate as the P1 operating point. Results of this analysis were judged to be representative of the experimental configuration at P1, because the alteration of the blade ratio (about 2%) was considered to be negligible in a subsonic flow regime, such as the present one, relying on experience (Arnone and Pacciani [24]).

Steady and unsteady characteristic curves of mass-averaged total pressure and Mach number at sections 7*M* and 8*M* are reported in Figs. 7 and 8 for both *G*2 and *G*5 geometries. Unsteady effects are not relevant for both geometries. Nevertheless, although negligible for *G*2, a slightly positive impact is observed on *G*5. For this geometry, an increase in total pressure at section 8*M* is found at P1 with respect to steady results (Fig. 7b). Considering the Mach number, which is

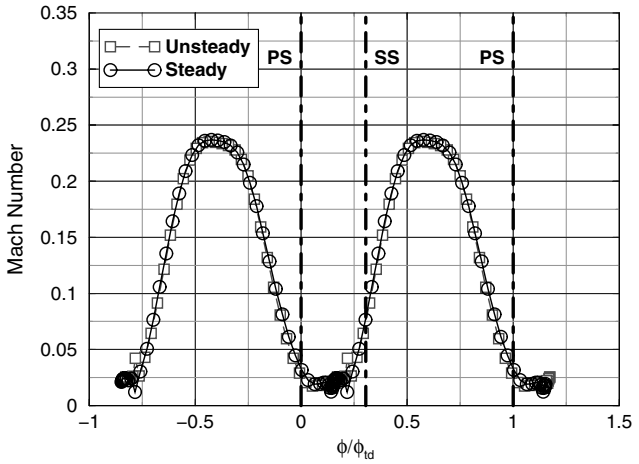

a) Section 7M

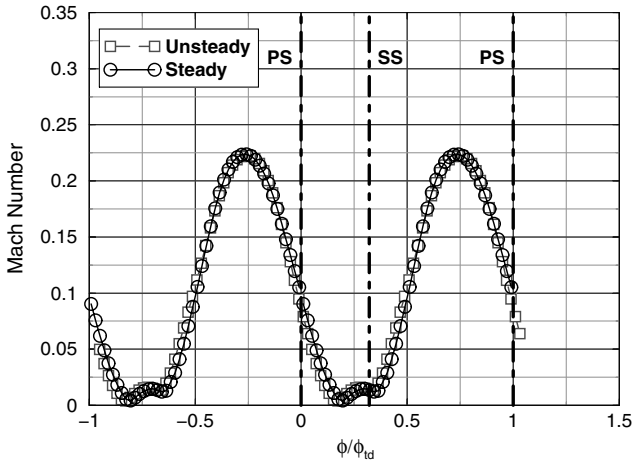

b) Section 8M

Fig. 9 Comparison between computed steady and time-averaged unsteady pitchwise distributions of spanwise-averaged Mach number at section 7*M* and 8*M* (P1, *G*2 geometry, approximate configuration).

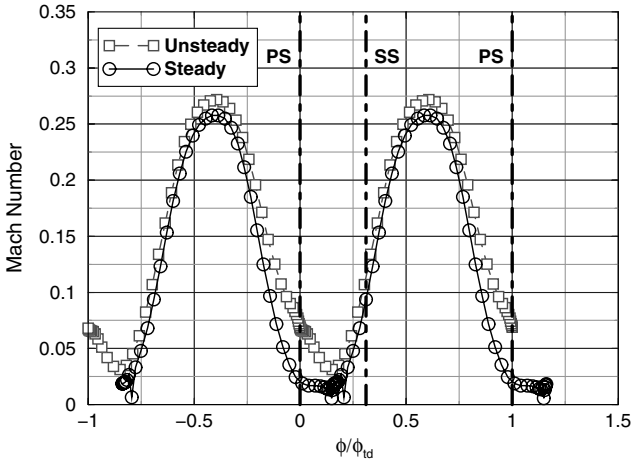

a) Section 7M

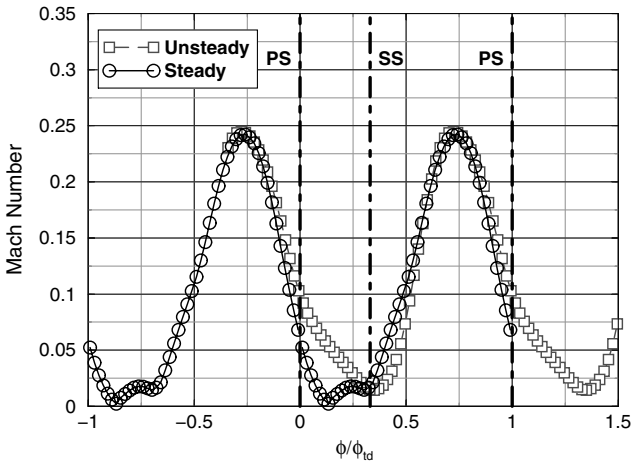

b) Section 8M

Fig. 10 Comparison between computed steady and time-averaged unsteady pitchwise distributions of spanwise-averaged Mach number at section 7*M* and 8*M* (P1, *G*5 geometry, approximate configuration).

related to the static pressure recovery inside the diffuser, at section 7*M*, both steady and unsteady analyses predict a higher level for *G*5 with respect to *G*2 (Fig. 8a). However, at section 8*M*, unsteady effects lower the Mach number for *G*5 to a value comparable to *G*2 (Fig. 8b). This result suggests that a more effective diffusion process occurs between sections 7*M* and 8*M* due to flow unsteadiness.

Further comparisons between steady and unsteady results are reported in terms of pitchwise distributions of spanwise mass-averaged Mach number and total pressure for *G*2 and *G*5 geometries. The absence of relevant unsteady effects on the flowfield downstream of the G2 diffuser vanes is assessed by Mach number distributions at sections 7*M* and 8*M* (Fig. 9). Similar results were obtained for total pressure distributions, not shown here. Considering the *G*5 geometry, major differences are observed in the wake region both at section 7*M* and 8*M* (Figs. 10 and 11). In particular, unsteady analysis predicts a narrower wake width with a more energized flow on the pressure side (Figs. 10a and 10b), and more homogeneous total pressure distributions (Figs. 11a and 11b) than the steady one. This result shows that flow unsteadiness determines a more uniform flowfield for *G*5 not only downstream of the diffuser vanes, as previously observed, but also inside vanes.

The analysis of diffuser blade pressure distributions for both geometries, reported in Fig. 12 at 50% span height, provides useful information about the diffusion process inside vanes. Again, no unsteady effects are visible on *G*2 (Fig. 12a). As concerning *G*5 (Fig. 12b), different blade loadings are predicted by steady and unsteady computations. In particular, although marginal differences are also present on the suction side close to the leading edge, the most significant ones are observed in the aft part of the vane. An overloading of the suction side from about 50% blade chord on, coupled with an unloading of the pressure side from 65% on, is predicted by unsteady analysis with respect to the steady one, so that at about 83% chord, the blade load is reversed. As a consequence, the time-averaged unsteady blade loading in the rear part of the diffuser vane is lower than the steady one. This result is found all over the span height.

Flow structure in the diffuser was investigated by looking at the flow streamlines, obtained by means of particle traces. In Figs. 13 and 14, streamlines in the blade-to-blade plane at midspan and in the meridional channel near pressure side are shown for both *G*2 and *G*5 geometries, together with Mach number contours. As far as blade-to-blade streamlines are concerned (Figs. 13 and 14, top), four vanes of the same geometry are reproduced: the two on the left show unsteady results, whereas the two on the right show steady ones. Downstream of the diffuser vanes, a wide low-Mach number wake is observed in all geometries and computations. No significant differences are found between steady and unsteady streamlines for *G*2 (Fig. 13, top), with a recirculating flow predicted by both analyses. This behavior is observed at all span heights. Otherwise, unsteady effects have a significant impact on *G*5 flow pattern (Fig. 14, top) because, unlike steady results, unsteady analysis predicts a nonrecirculating wake flow. The blade-to-blade streamline pattern at other span heights, not reported here, shows that recirculations are suppressed from about 50% span on. Moreover, the extent of the recirculating region from midspan down to the rear wall is lower in unsteady results than in steady ones. Significant differences are also observed in the vaned

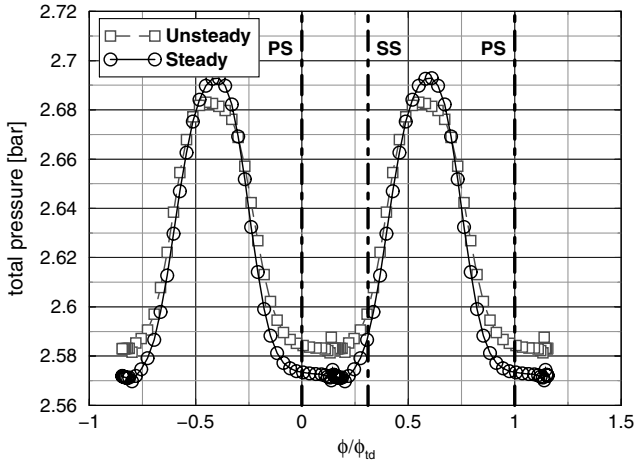

a) Section 7M

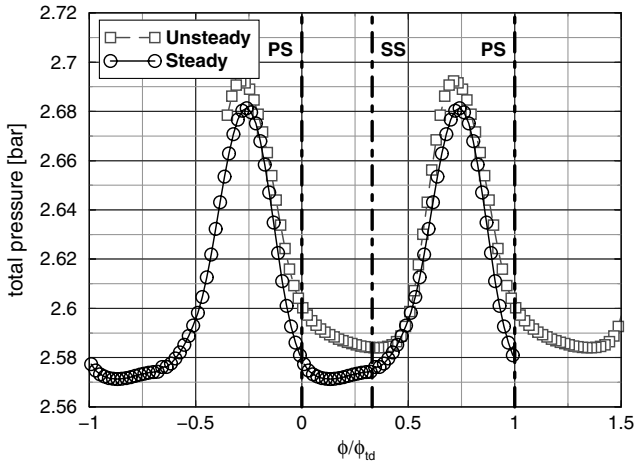

b) Section 8M

Fig. 11 Comparison between computed steady and time-averaged unsteady pitchwise distributions of spanwise-averaged total pressure at section 7*M* and 8*M* (P1, *G*5 geometry, approximate configuration).

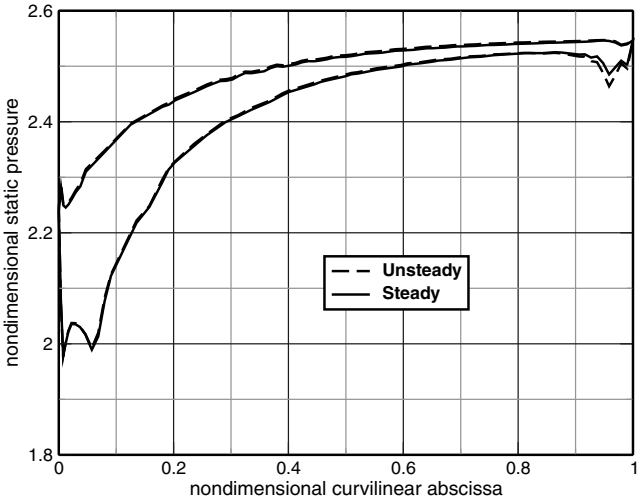

a) 50% span – G2

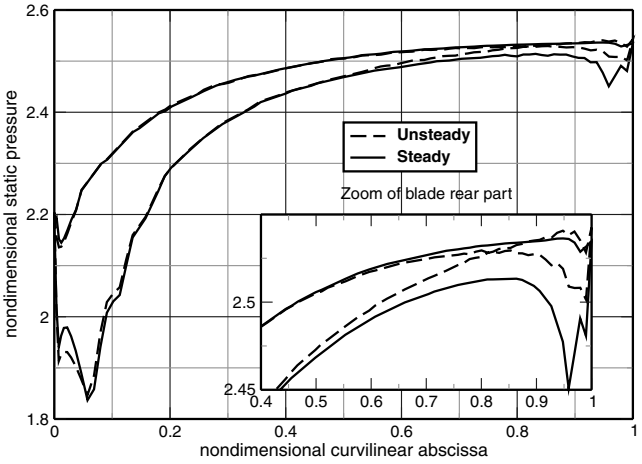

b) 50% span – G5

Fig. 12 Comparison between steady and time-averaged unsteady diffuser blade pressure distributions (P1, approximate configuration).

space. In particular, steady analysis predicts a thin separation bubble on the pressure side extending from about 50% of the chord to the trailing edge. This bubble has totally disappeared in the unsteady one. This result is determined by the unloading of the aft part of the diffuser vane, as previously discussed (Fig. 12b). Meridional streamlines close to the pressure side highlight that the steady separation is completely suppressed by flow unsteadiness all over the span (Fig. 14, bottom). This is not the case for *G*2 geometry, where the separation is still maintained in unsteady results (Fig. 13, bottom). It is worth noticing that this result is in agreement with Peeters and Sleiman [17], who found significantly less separation in the unsteady analysis of a vaned diffuser for a different centrifugal stage.

Previous results assessed a beneficial impact of unsteady effects on the *G*5 diffuser performance and flowfield. To understand the physical mechanisms responsible for this behavior, which are triggered by unsteady impeller–diffuser interaction, a more in-depth analysis of the diffuser flowfield was carried out.

In Fig. 15, steady and time-averaged unsteady distributions of nondimensional entropy and secondary vorticity (SV) are shown at five crossflow planes inside *G*5 vanes. In each figure, steady plots are reported on the left vane, whereas unsteady results are depicted on the right one.

As far as entropy distributions are concerned (Fig. 15a), near the diffuser leading edge (plane 1), major losses are located close to the shroud region for both steady and unsteady results, according to the impeller jet-wake model. However, different evolutions of losses are observed inside the vanes (planes 2–5). In steady results, high-loss regions are localized near the pressure side, consistent with the presence of recirculating flow (Fig. 14, bottom). Low-loss flow is shifted from the center of the channel toward the suction side. Otherwise, a more centered low-loss flow is predicted by unsteady analysis, with high-loss regions more uniformly split on pressure and suction sides.

Secondary vorticity is defined as the vorticity component orthogonal to the considered crossflow planes:

$$\mathrm{SV} \equiv \nabla \times \boldsymbol{c} \cdot \boldsymbol{n} \tag{1}$$

here, $\boldsymbol{c}$ is the time-averaged local velocity and $\boldsymbol{n}$ is the unit vector normal to each crossflow plane and downstream oriented. The sign of SV determines the rotational direction. Looking at the figure, positive values of SV correspond to vortices rotating in the counterclockwise direction, and negative values indicate clockwise rotation. Crossflow distributions of SV, reported in Fig. 15b, show relevant differences between steady and unsteady results throughout the vane (planes 1–5). In both cases, high positive SV regions are approximately located in the upper 50% of span height. However, in unsteady results, these regions are more pronounced and extend closer to the vane pressure side (planes 2–5). This more positive pressure side SV, originating from the impeller wake and showing counterclockwise vortices, is the physical mechanism which moves the high-energy core flow from suction to pressure side, unloading it and preventing separation. This result is in agreement with the hypothesis proposed by Ziegler et al. [19] about the presence of a

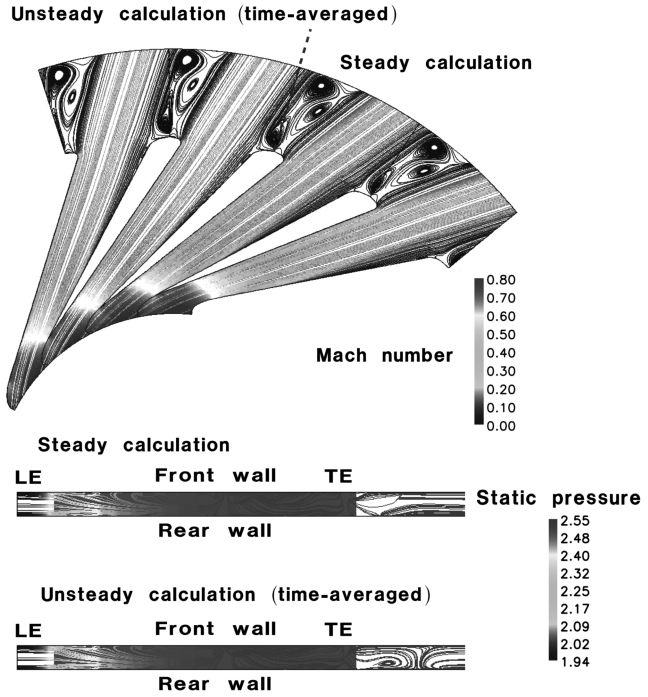

Fig. 13 Comparison between computed steady and time-averaged unsteady diffuser streamlines, Mach number at midspan (top), and static pressure contours near the pressure side (bottom) (P1, *G*2 geometry, approximate configuration).

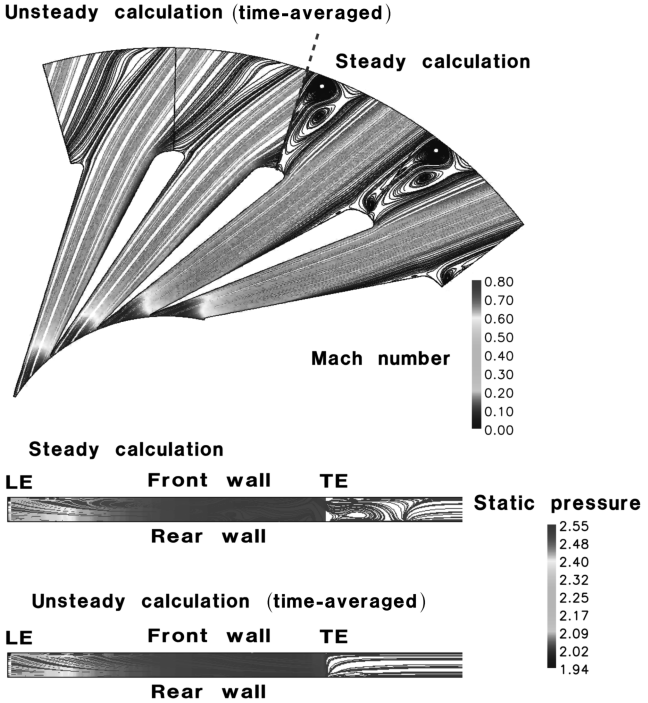

Fig. 14 Comparison between computed steady and time-averaged unsteady diffuser streamlines, Mach number at midspan (top), and static pressure contours near the pressure side (bottom) (P1, *G*5 geometry, approximate configuration).

strong vortex in the diffuser throat helping the vane pressure side not to separate.

V. Conclusions

Impeller–diffuser interaction is known to have a relevant impact on the performance and the flowfield of heavily loaded centrifugal compressor stages. For this reason, considerable efforts were and are currently being devoted to improve the understanding of this phenomenon. In this work, two diffuser geometries of the open test case Radiver, differing in the radial gap between impeller exit and diffuser inlet, were analyzed by means of both steady and unsteady computations with the aim of separating unsteady effects from steady ones. The following conclusions were reached:

1) Numerical predictions were assessed using the good agreement observed between experimental and numerical results, in terms of both characteristic curves and distributions of the main fluid-dynamic quantities.

2) Flow unsteadiness marginally affects the stage performance, but it has a relevant impact on the flowfield. Even if the interaction mainly occurs in the radial gap region, its time-average effects are more evident downstream, helping the flow on the diffuser pressure side not to separate in the minimum radial gap geometry.

3) The physical mechanism by which unsteady interaction affects the flowfield was identified in the structure of vortices in crossflow planes, highlighted by secondary vorticity distributions. These vortices, originating from the impeller wake, affect the diffusion process by moving the high-energy core flow from suction to pressure side.

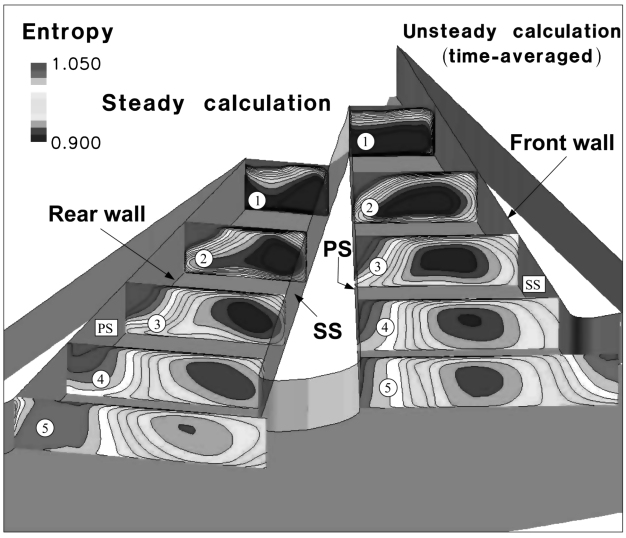

a) Specific entropy

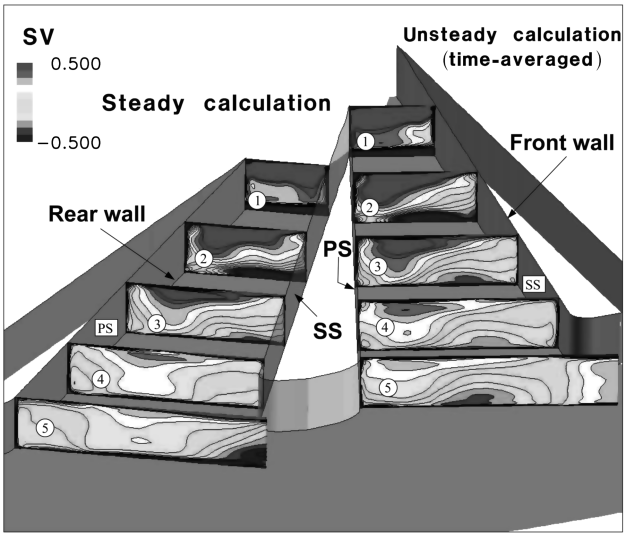

b) Secondary vorticity

Fig. 15 Comparison between computed steady and time-averaged unsteady distributions of nondimensional entropy and secondary vorticity at different crossflow planes (P1, *G*5 geometry, approximate configuration).

As a final consideration, the experimental evidence of the better performance of the lower radial gap stage at the collector exit is explained by the more regular (i.e., nonrecirculating) flow pattern observed at the diffuser exit.

Acknowledgments

The authors would like to thank Kai U. Ziegler, and Reinhard Niehuis and his staff at the Institute of Jet Propulsion and Turbomachinery of the RWTH Aachen University, Germany, University of Technology, for providing the Radiver test case, and for the fruitful discussions.

References

[1] Bonaiuti, D., Arnone, A., Hah, C., and Hayami, H., "Development of Secondary Flow Field in a Low Solidity Diffuser in a Transonic Centrifugal Compressor Stage," American Society of Mechanical Engineers Paper GT-2002-30371, 2002.

[2] Ibaraki, S., Matsuo, T., Kuma, H., Sumida, K., and Suita, T., "Aerodynamics of a Transonic Centrifugal Compressor Impeller," American Society of Mechanical Engineers Paper GT-2002-30374, 2002.

[3] Hayami, H., Hojo, M., Hirata, N., and Aramaki, S., "Flow with Shock Waves in a Transonic Centrifugal Compressor with a Low-Solidity Cascade Diffuser Using PIV," American Society of Mechanical Engineers Paper GT2004-53268, 2004.

[4] Higashimori, H., Hasagawa, K., Sumida, K., and Suita, T., "Detailed Flow Study of Mach Number 1.6 High Transonic Flow with a Shock Wave in a Pressure Ratio 11 Centrifugal Compressor Impeller," American Society of Mechanical Engineers Paper GT2004-53435, 2004.

[5] Gottfried, D., and Fleeter, S., "Impeller Blade Unsteady Aerodynamic Response to Vaned Diffuser Potential Fields," *Journal of Propulsion and Power*, Vol. 18, No. 2, March–April 2002, pp. 472–480.

[6] Rodgers, C., "The Performance of Centrifugal Compressor Channel Diffusers," American Society of Mechanical Engineers Paper 82-GT-10, 1982.

[7] Clements, W., and Artt, D., "The Influence of Diffuser Vane Leading Edge Geometry on the Performance of a Centrifugal Compressor," American Society of Mechanical Engineers Paper 89-GT-163, 1989.

[8] Sanders, A. J., and Fleeter, S., "Potential Field Interactions in a Low-Speed Centrifugal Compressor," *Journal of Propulsion and Power*, Vol. 14, No. 6, Nov.–Dec. 1998, pp. 925–933.

[9] Shum, Y. K. P., Tan, C. S., and Cumpsty, N. A., "Impeller-Diffuser Interaction in a Centrifugal Compressor," *Journal of Turbomachinery*, Vol. 122, No. 4, Oct. 2000, pp. 777–786. doi:10.1115/1.1308570

[10] Filipenco, V. G., Deniz, S., Johnston, J. M., Greitzer, E. M., and Cumpsty, N. A., "Effects of Inlet Flow Field Conditions on the Performance of Centrifugal Compressor Diffusers, Part 1: Discrete-Passage Diffuser," *Journal of Turbomachinery*, Vol. 122, No. 1, Jan. 2000, pp. 1–10. doi:10.1115/1.555418

[11] Deniz, S., Greitzer, E. M., and Cumpsty, N. A., "Effects of Inlet Flow Field Conditions on the Performance of Centrifugal Compressor Diffusers, Part 2: Straight-Channel Diffuser," *Journal of Turbomachinery*, Vol. 122, No. 1, Jan. 2000, pp. 11–21. doi:10.1115/1.555424

[12] Krain, H., "A Study on Centrifugal Impeller and Diffuser Flow," *Journal of Engineering for Power*, Vol. 103, No. 4, 1981, pp. 688–697.

[13] Krain, H., *Experimental Observations of the Flow in Impellers and Diffusers*, VKI Lecture Series, Vol. 1984-07, von Kármán Inst. for Fluid Dynamics, Rhode Saint Genese, Belgium, 1984.

[14] Inoue, M., and Cumpsty, N. A., "Experimental Study of Centrifugal Impeller Discharge Flow in Vaneless and Vaned Diffusers," *Journal of Engineering for Gas Turbines and Power*, Vol. 106, No. 2, 1984, pp. 455–467.

[15] Ibaraki, S., Matsuo, T., and Yokoyama, T., "Investigation of Unsteady Flow Field in Vaned Diffuser of a Transonic Centrifugal Compressor," American Society of Mechanical Engineers Paper GT2006-90268, 2006.

[16] Sanders, A. J., and Fleeter, S., "Blading Response to Potential Field Interactions in Axial- and Radial- Flow Turbomachinery," *Journal of Propulsion and Power*, Vol. 14, No. 2, March–April 1998, pp. 199–207.

[17] Peeters, M., and Sleiman, M., "A Numerical Investigation of the Unsteady Flow in Centrifugal Stages," American Society of Mechanical Engineers Paper 2000-GT-426, 2000.

[18] Ziegler, K. U., Gallus, H. E., and Niehuis, R., "A Study on Impeller-Diffuser Interaction, Part 1: Influence on the Performance," *Journal of Turbomachinery*, Vol. 125, No. 1, Jan. 2003, pp. 173–182. doi:10.1115/1.1516814

[19] Ziegler, K. U., Gallus, H. E., and Niehuis, R., "A Study on Impeller-Diffuser Interaction, Part 2: Detailed Flow Analysis," *Journal of Turbomachinery*, Vol. 125, No. 1, Jan. 2003, pp. 183–192. doi:10.1115/1.1516815

[20] Ziegler, K. U., "Experimentelle Untersuchung der Laufrad-Diffusor-Interaktion in einem Radialverdichter variabler Geometrie," Ph.D. Thesis, RWTH Aachen Univ., Germany, 2003.

[21] Arnone, A., Liou, M. S., and Povinelli, L. A., "Multigrid Calculation of Three-Dimensional Viscous Cascade Flows," *Journal of Propulsion and Power*, Vol. 9, No. 4, July–Aug. 1993, pp. 605–614.

[22] Arnone, A., "Viscous Analysis of Three-Dimensional Rotor Flow Using a Multigrid Method," *Journal of Turbomachinery*, Vol. 116, July 1994, pp. 435–445.

[23] Jameson, A., "Time Dependent Calculations Using Multigrid with Applications to Unsteady Flows past Airfoils and Wings," *10th Computational Fluid Dynamics Conference*, AIAA Paper 91-1596, 1991.

[24] Arnone, A., and Pacciani, R., "Rotor-Stator Interaction Analysis Using the Navier–Stokes Equations and a Multigrid Method," *Journal of Turbomachinery*, Vol. 118, No. 4, Oct. 1996, pp. 679–689.

[25] Baldwin, B. S., and Lomax, H., "Thin Layer Approximation and Algebraic Model for Separated Turbulent Flows," AIAA Paper 78-257, 1978

[26] Arnone, A., and Pacciani, R., "IGV-Rotor Interaction Analysis in a Transonic Compressor Using the Navier–Stokes Equations," *Journal of Turbomachinery*, Vol. 120, No. 1, 1998, pp. 147–155.

[27] Spalart, P., and Allmaras, S., "A One-Equation Turbulence Model for Aerodynamic Flows," AIAA Paper 92-0439, 1992.

[28] Menter, F. R., "Zonal Two-Equations $k-\omega$ Turbulence Models for Aerodynamic Flows," AIAA Paper 93-2906, 1993.

[29] Arnone, A., Bonaiuti, D., Boncinelli, P., Ermini, M., Milani, A., Baldassarre, L., and Camatti, M., "CFD Applications to Industrial Centrifugal Compressor Design," American Society of Mechanical Engineers Paper GT-2002-30393, 2002.

[30] Weiss, C., Grates, D. R., Thermann, H., and Niehuis, R., "Numerical Investigation of the Influence of the Tip Clearance on Wake Formation Inside a Radial Impeller," American Society of Mechanical Engineers Paper GT2003-38279, 2003.

F. Liu
Associate Editor